Materials Advances

ROYAL SOCIETY OF CHEMISTRY

COMMUNICATION

View Article Online
View Journal | View Issue

Cite this: *Mater. Adv.*, 2024, 5, 3173

Received 14th February 2024,
Accepted 18th March 2024

DOI: 10.1039/d4ma00147h

rsc.li/materials-advances

Modulation of Cu/Cu_2O nanoparticles to promote the photocurrent response for light-enhanced pseudocapacitive charge storage†

Jing Xie,[ab] Yuhao Zhong,[b] Weiting Meng,[b] Xiaobo Feng[bc] and Ting Zhu *[bc]

Copper metal/copper oxide (Cu/Cu_2O) hybrid nanoparticles (HNPs) were grown on carbon cloth by an electrodeposition method. The ratio of Cu_2O in these HNPs was increased by calcination in air, remarkably promoting the photocurrent response by 150%. This CC@Cu/Cu_2O photoelectrode delivered a high specific capacitance of 166 mF cm^{-2} (at 5 mA cm^{-2}) under light irradiation, exhibiting a light enhancement of 17.7%. In addition, a high retention of 92% can be achieved after 5000 cycles with light.

The energy shortage and environmental problems have prompted human beings to search for green and sustainable energy sources, like solar energy.[1–3] In the past few years, solar cells have been considered one of the most important technologies for direct utilization of solar energy due to their low cost, easy manufacturing, and high efficiency of solar-to-electricity conversion.[4–6] However, the intermittence and variability of sunlight is the main challenge to harvest and convert solar energy efficiently. Therefore, advanced energy storage devices have been developed to connect with solar cells for conversion and storage of solar energy by directly charging the energy devices.[7] For example, Wang *et al.* demonstrated a pioneering work by incorporating a dye-sensitized solar cell (DSSC) and a lithium ion battery (LIB) on the same Ti foil that had double-sided TiO_2 nanotube (NTs) arrays, and this power pack can deliver a discharge capacity of 38.89 μA h under 100 μA with a light efficiency of 0.82%.[8] Later, Dai *et al.* employed perovskite solar cell packs for direct charging of LIBs, delivering a high overall photo-electric conversion and storage efficiency of 7.80%.[9] However, these power packs usually contain two separate parts, namely sunlight harvesting/conversion and electricity storage, which requires a large volume of package with external conductive connections. In recent years, bifunctional photoelectrodes have been developed to realize the *in situ* harvesting and storage of solar energy, largely enhancing the charge storage and light efficiency.[10–13] Jiang *et al.* reported a light-motivated SnO_2/TiO_2 heterojunction for LIBs, which enhanced the lithiation kinetics and electrochemical reversibility of both SnO_2 and TiO_2.[14] As a result, the specific capacity can be increased from 1.91 to 3.47 mA h cm^{-2} at 5 mA cm^{-2} for the as-reported SnO_2/TiO_2 anodes. In such bifunctional photoelectrodes, the key challenge is to optimize these two kinds of materials on an atomic scale for efficient charge separation and migration.

Pseudocapacitive energy devices employing faradaic reactions of transition metal oxides/sulfides show similar energy storage mechanisms with battery technology,[15] but usually deliver much higher power density and longer cycling life than LIBs,[16] thus serving as an important alternative to batteries.[17] Photoactive materials, such as TiO_2, Fe_2O_3, Co_3O_4, ZnO, *etc.* were selected as photoelectrodes to accelerate the photoinduced charge carriers.[18–22] During the charging process, the photogenerated electrons transfer to the conduction bands, which are circulated with the external electron flux, while the photogenerated holes left in the valence bands can participate in the oxidation reaction for an additional charge storage within the electrodes.[23] However, it is still a big challenge to balance the strong photosensitivity, good electroactivity and high electric conductivity within a single electrode.[24] Herein, pseudocapacitive electrode materials with high photoactivity and conductivity composed of Cu/Cu_2O HNPs were prepared by a facile electrodeposition method against carbon cloth (CC) substrates. CC was used herein due to its high electric conductivity and good flexibility that is favorable to the electrochemical performance. The content ratio of Cu_2O in this photoelectrode material (CC@Cu/Cu_2O) can be increased by a subsequent calcination in air, further enhancing the photo responsive capability of this photoelectrode. Due to the strong photosensitivity and electroactivity of Cu_2O, and good high conductivity of Cu metal and CC, the typical CC@Cu/Cu_2O

[a] *School of Materials Science and Engineering, Central South University, 932 Lushan Road South, Changsha 410083, Hunan, China*
[b] *School of Physics and Electronic Information, Yunnan Normal University, 768 Juxian Street, Kunming 650500, Yunnan, China. E-mail: zhut0002@ynnu.edu.cn*
[c] *Yunnan Key Laboratory of Optoelectronic Information Technology, Yunnan Normal University, Kunming 650500, Yunnan, China*

† Electronic supplementary information (ESI) available. See DOI: https://doi.org/10.1039/d4ma00147h

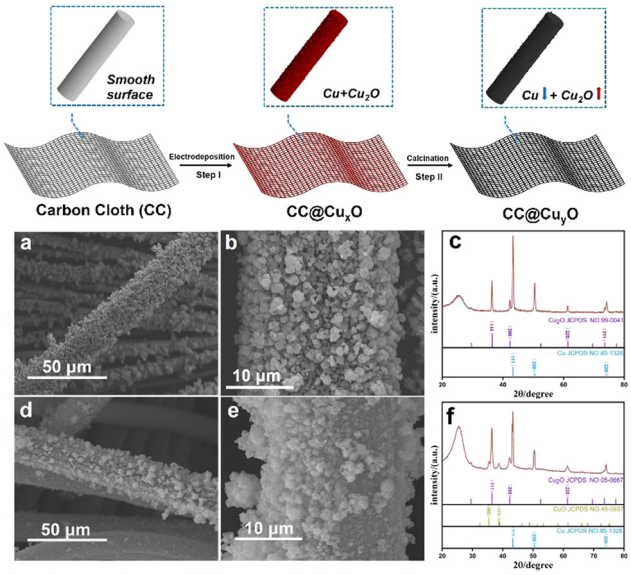

Fig. 1 Schematic illustration of the synthetic process (top image), and SEM (a), (b), (d), and (e) and XRD patterns (c) and (f) of the CC@Cu_xO (a)–(c) and CC@Cu_yO (d)–(f) samples.

($CC@Cu_yO$) photoelectrode delivered a high specific capacitance of 166 F cm^{-2} at 5 mA cm^{-2} for pseudocapacitive charge storage under light irradiation, calculating a remarkable light enhancement of 17.7% compared to that obtained without light. In addition, this CC@Cu/Cu_2O photoelectrode exhibited a capacitance retention of 92% after 5000 cycles under light on conditions, suggesting a good photo and electrochemical stability.

The synthetic strategy for the CC@Cu/Cu_2O samples is presented in Fig. 1 (top image). The bare CC was firstly treated in HNO_3 aqueous solution before being rinsed by DI water and dried at 70 °C for 10 h. The hydrophilicity of the CC after acid treatment is largely improved (Fig. S1, ESI†). The high surface hydrophilicity of CC can endow a good contact with charged ions in aqueous solution, which may lead to efficient and homogeneous deposition of Cu/Cu_2O species. The CC after acid treatment was then used as a growth substrate for the direct electrodeposition of Cu_xO (step I) HNPs, forming one-dimensional (1D) CC@Cu/Cu_2O hybrid structures. A subsequent calcination in air of this CC@Cu/Cu_2O leads to the oxidation of Cu metals (step II), generating more Cu_2O within the particles (Cu_yO). The morphologies of CC@Cu_xO before calcination are shown by the SEM results (Fig. 1a and b), where a rough surface against the 1D structures can be clearly observed. Compared to the bare CC, the average diameter of these 1D structures is increased to 25 μm. After annealing, the average diameter of the 1D structures is almost unchanged, while more particles have been aggregated into larger sizes (Fig. 1d and e). The particle sizes of Cu_xO were increased after calcination due to aggregation caused by re-crystallization during the heat treatment. The XRD patterns (Fig. 1c *vs.* Fig. 1f) show that the peak intensity of Cu (111) has reduced remarkably after calcination compared to Cu_2O (111) and CuO (111), revealing that more Cu species were transformed into Cu_2O/CuO. This also suggests that the content ratio of Cu_2O has been increased after annealing treatment, which results from the oxidation of more Cu metals during the calcination process.

To further examine the structural and elemental information of the Cu/Cu_2O HNPs, TEM and elemental mappings were conducted to compare the samples before and after calcination. Fig. 2a shows a TEM image of the Cu_xO aggregates, which were collected by ultrasonication from a substrate. The identified lattices of 0.208 and 0.246 nm from the HR-TEM image (Fig. 2b) can be assigned to the Cu (111) and Cu_2O (111), respectively.[25] Moreover, the elemental mapping results shown in Fig. 2c and d have demonstrated that the Cu and O elements are homogeneously interspersed, confirming the co-formation of Cu and Cu_2O during the electrodeposition. After annealing, the lattices of Cu (111) and Cu_2O (111) can be distinguished explicitly (Fig. 2e), while the lattice of CuO is absent, which should be due to a very low content within the particles. In addition, similar elemental distributions of Cu and O can be seen after annealing, verifying the uniform distribution of Cu and Cu_2O.

To examine the chemical status of copper elements in the as-prepared Cu/Cu_2O HNPs, XPS was performed and compared in Fig. 3a and b. Before calcination, only Cu^+ can be detected in the Cu_xO sample, which corresponds to the binding energies of 952.61 eV (Cu $2p_{1/2}$) and 932.77 eV (Cu $2p_{3/2}$),[26] respectively (Fig. 3a). Meanwhile, both Cu^+ and Cu^{2+} can be detected in the Cu_yO sample after calcination, which can be seen in Fig. 3b. The binding energies of 955.5 and 936.2 eV can be assigned to Cu $2p_{1/2}$ and Cu $2p_{3/2}$ of Cu^{2+}, respectively. The presence of Cu^{2+} should be due to a slight and partial oxidation of Cu_2O during the calcination at 300 °C. Moreover, the bind energies of Cu^+ have been shifted positively to 953.5 eV (Cu $2p_{1/2}$) and 934.1 eV (Cu $2p_{3/2}$), which could be caused by the oxidation of more Cu. It has been reported that there is a good photo responsive property of Cu_2O,[27] and thus the photocurrent responses were measured for the CC@Cu_xO and CC@Cu_yO samples. Upon light irradiation, there is a steady photocurrent of ~0.12 mA cm^{-2} for the CC@Cu_xO sample, and the current can be increased to ~0.3 mA cm^{-2} for the CC@Cu_yO sample (Fig. 3c), revealing a better photoactivity of the sample with higher ratio of Cu_2O and CuO. The higher photocurrent

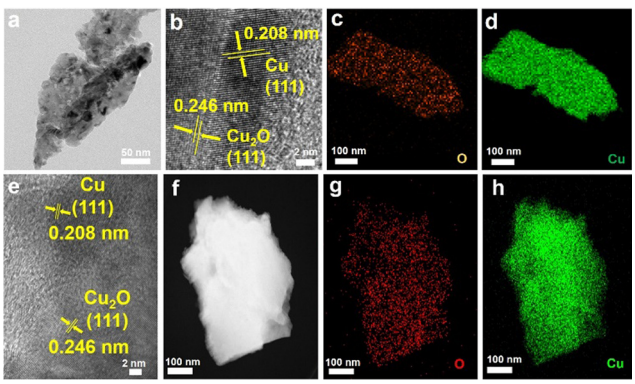

Fig. 2 TEM images (a), (b), and (e), HAADF-TEM (f), and elemental mappings (c), (d), (g), and (h) of the CC@Cu_xO (a)–(d) and CC@Cu_yO (e)–(h) samples.

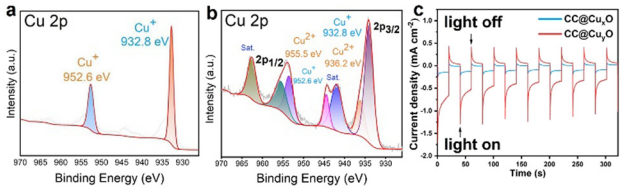

Fig. 3 XPS spectrum of Cu 2p (a) and (b) and photocurrent response (c) of the CC@Cu_xO (a) and blue curve in (c) and CC@Cu_yO (b) and red curve in (c) samples.

response should be mainly contributed by Cu_2O, as Cu_2O is reported to exhibit much better photocurrent response than CuO.[28] In addition, the content ratio of CuO is tiny in the as-prepared Cu/Cu_2O particles, which played a minor role in the increase of photocurrent response.

The electrochemical surface area (ECSA) is also significant for electrochemical charge storage, and thus non-faradaic CV measurements were performed for the CC, CC@Cu_xO, and CC@Cu_yO samples, respectively (Fig. S2, ESI†). The calculated double-layer capacitances for all three samples are 0.9, 27.8, and 61.5 mF cm^{-2}, revealing the highest ECSA value of the CC@Cu_yO sample. A higher ECSA is considered favorable to store more charged ions at the electrode–electrolyte interface.[29]

Next, the as-prepared CC@Cu/Cu_2O samples were then directly employed as electrodes for pseudocapacitive charge storage. Fig. 4 displays the CV, GCCD and cycling performance curves of the CC@Cu_yO sample (note: a broader voltage window of 0–0.6 V was applied for CV measurements to contain all the redox peaks). A remarkable CV areal enlargement can be seen from the comparison of the light on and off conditions at 50 mV s^{-1} (Fig. 4a), verifying the light-enhancement of the sample. In addition, higher current densities under light on conditions were delivered than those of the respective light off conditions, which can be found from the CV curves in Fig. 4b and c, respectively. During the charge–discharge process, a longer GCCD time can be delivered

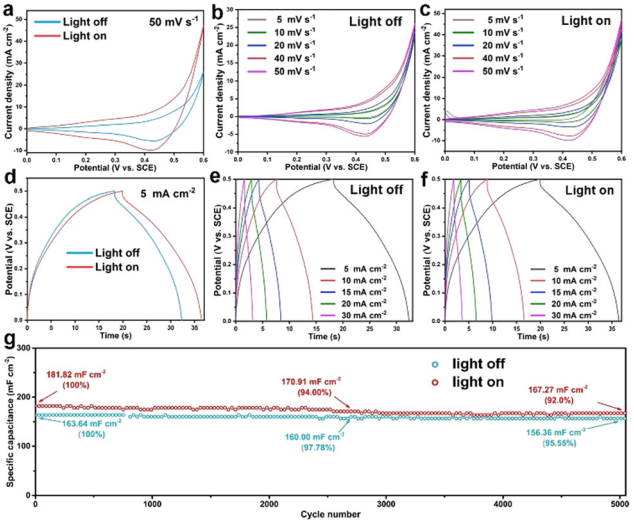

Fig. 4 CV curves (a)–(c), GCCD curves (d)–(f), and cycling performance (g) of the CC@Cu_yO sample under light on and off conditions, respectively.

for the light on conditions than those for the light off conditions (Fig. 4d–f). A discharge specific capacitance of 141 mF cm^{-2} can be calculated at 5 mA cm^{-2} under light off conditions, and the capacitance was increased to 166 mF cm^{-2} under light on conditions (Fig. 4d), revealing a light enhancement of 17.7%. While for the CC@Cu_xO sample, there are no remarkable differences for the CV and GCCD results under light off and on conditions (Fig. S3, ESI†), respectively, suggesting that the higher ratios of Cu_2O in the CC@Cu_yO sample derived from the calcination may promote the pseudocapacitive property.

As a comparison, CV and GCCD measurements were also carried out for the bare CC sample, and the results are shown in Fig. S4 (ESI†), where a negligible CV loop and GCCD time can be recoded, revealing the negligible capacitive contribution from the CC substrate. To evaluate the cycling stability of the CC@Cu_yO sample, the long-term test was carried out at 2 mA cm^{-2} for 5000 cycles under light off and on conditions, respectively (Fig. 4g). Initial specific capacitances of 163.64 and 181.82 mF cm^{-2} can be calculated for the light off and on conditions, respectively, while the capacitances were decreased to 156.36 and 167.27 mF cm^{-2} after 5000 cycles, revealing the capacitance retentions of 95.55% and 92%, respectively. The slightly higher decay of the light on condition should be caused by possible photo corrosion of Cu_2O during the cycling test. However, it should be noted that the cycling performance of the light on condition is comparable to the light off condition, which again validated a good stability of the CC@Cu_yO electrode under light irradiation.

In summary, carbon cloth-supported Cu/Cu_2O HNPs were prepared by an electrodeposition/calcination method. The ratio of Cu_2O in the sample can be increased after calcination in air, leading to a remarkably increased photocurrent response by 150%. As a result, the CC@Cu_yO sample with higher ratio of Cu_2O has exhibited a high specific capacitance of 166 mF cm^{-2} under light irradiation, delivering a light enhancement of 17.7% compared to that obtained without light. In addition, a high capacitance retention of 92% can be achieved after 5000 cycles under light irradiation, revealing a good cycling stability of the sample. As a comparison, the cycling performances of the CC@Cu_xO sample were also evaluated under light off and on conditions (Fig. S5, ESI†), where lower specific capacitances with quick decay were obtained. This work may provide a new pathway to improve the pseudocapacitive charge storage for the typical metal oxide-based pseudocapacitive materials.

J. Xie and Y. H. Zhong carried out the experiments and analysed the collected data, W. T. Meng helped in the material characterization, T. Zhu conceived the research idea, supervised the project and wrote the manuscript, and X. B. Feng provided a discussion and revised the manuscript.

This work is financially supported by the National Natural Science Foundation of China (grant No. 52263028) and the Yunnan Fundamental Research Projects (grant No. 202301AT070059).

Conflicts of interest

The authors declare no competing financial interest.

Notes and references

1 A. J. Carrillo, J. González-Aguilar, M. Romero and J. M. Coronado, *Chem. Rev.*, 2019, **119**, 4777–4816.
2 X. F. Zhang, W. H. Huang, L. Yu, M. García-Melchor, D. S. Wang, L. J. Zhi and H. B. Zhang, *Carbon Energy*, 2023, e362.
3 W. H. Huang, T. T. Bo, S. W. Zuo, Y. Z. Wang, J. M. Chen, S. Ould-Chikh, Y. Li, W. Zhou, J. Zhang and H. B. Zhang, *Susmat*, 2022, **2**, 466–475.
4 Y. Y. Zhou, L. M. Herz, A. K. Y. Jen and M. Saliba, *Nat. Energy*, 2022, **7**, 794–807.
5 L. P. Duan, D. Walter, N. T. Chang, J. Bullock, D. Kang, S. P. Phang, K. Weber, T. White, D. Macdonald, K. Catchpole and H. P. Shen, *Nat. Rev. Mater.*, 2023, **8**, 261–281.
6 H. F. Yao and J. H. Hou, *Angew. Chem., Int. Ed.*, 2022, **61**, e202209021.
7 J. Bae, Y. J. Park, M. Lee, S. N. Cha, Y. J. Choi, C. S. Lee, J. M. Kim and Z. L. Wang, *Adv. Mater.*, 2011, **23**, 3446–3449.
8 W. X. Guo, X. Y. Xue, S. H. Wang, C. J. Lin and Z. L. Wang, *Nano Lett.*, 2012, **12**, 2520–2523.
9 J. T. Xu, Y. H. Chen and L. M. Dai, *Nat. Commun.*, 2015, **6**, 8103.
10 O. Nguyen, E. Courtin, F. Sauvage, N. Krins, C. Sanchez and C. Laberty-Robert, *J. Mater. Chem. A*, 2017, **5**, 5927–5933.
11 K. Shimokawa, S. Matsubara, A. Okamoto and T. Ichitsubo, *Chem. Commun.*, 2022, **58**, 9634–9637.
12 B. Deka Boruah and M. D. Volder, *J. Mater. Chem. A*, 2021, **9**, 23199–23205.
13 M. Zhang, L. Pan, Z. Jin, X. Wang, H. Mei, L. Cheng and L. Zhang, *Adv. Energy Mater.*, 2023, **13**, 2204058.
14 C. Hu, L. Chen, Y. J. Hu, A. P. Chen, L. Chen, H. Jiang and C. Z. Li, *Adv. Mater.*, 2021, **33**, 2103558.
15 C. H. An, Y. Q. Li, S. Wu, L. X. Gao, L. Y. Lin, Q. B. Deng and N. Hu, *Rare Met.*, 2023, **42**, 1959–1968.
16 J. Zhou, B. B. Liu, H. Zheng, W. Q. Ma, Q. Li and C. X. Xu, *Rare Met.*, 2023, **43**, 682–691.
17 P. Simon and Y. Gogotsi, *Nat. Mater.*, 2008, **7**, 845–854.
18 J. Xu, H. Wu, L. F. Lu, S. F. Leung, D. Chen, X. Y. Chen, Z. Y. Fan, G. Z. Shen and D. D. Li, *Adv. Funct. Mater.*, 2014, **24**, 1840–1846.
19 K. J. Zhu, G. X. Zhu, J. Wang, J. X. Zhu, G. Z. Sun, Y. Zhang, P. Li, Y. F. Zhu, W. J. Luo, Z. G. Zou and W. Huang, *J. Mater. Chem. A*, 2018, **6**, 21360–21367.
20 R. Sinha, N. Roy and T. K. Mandal, *Chem. Eng. J.*, 2022, **431**, 133915.
21 L. Q. Bai, H. W. Huang, S. G. Zhang, L. Hao, Z. L. Zhang, H. F. Li, L. Sun, L. N. Guo, H. T. Huang and Y. H. Zhang, *Adv. Sci.*, 2020, **7**, 2001939.
22 X. Wu, H. B. Zhang, S. W. Zuo, J. C. Dong, Y. Li, J. Zhang and Y. Han, *Nano-Micro Lett.*, 2021, **13**, 136.
23 Y. B. Zhao, H. Li, R. Y. Tang, X. Y. Wang, Y. Wu, S. Yan and Y. Zhang, *J. Mater. Chem. A*, 2023, **11**, 15844–15854.
24 N. Flores-Diaz, F. De Rossi, A. Das, M. Deepa, F. Brunetti and M. Freitag, *Chem. Rev.*, 2023, **123**, 9327–9355.
25 C. H. An, Z. F. Wang, W. Xi, K. Wang, X. Z. Liu and Y. Ding, *J. Mater. Chem. A*, 2019, **7**, 15691–15697.
26 Z. R. Shen, J. B. Yan, M. Wang, L. D. Xing, B. J. Huang, H. Y. Zhou, W. B. Li, L. S. Chen and J. L. Shi, *ACS Sustainable Chem. Eng.*, 2023, **11**, 9433–9441.
27 Y. A. Wu, I. McNulty, C. Liu, K. C. Lau, Q. Liu, A. P. Paulikas, C. J. Sun, Z. H. Cai, J. R. Guest, Y. Ren, V. Stamenkovic, L. A. Curtiss, Y. Z. Liu and T. Rajh, *Nat. Energy*, 2019, **4**, 957–968.
28 Y. H. Zhu, Z. W. Xu, K. Yan, H. B. Zhao and J. D. Zhang, *ACS Appl. Mater. Interfaces*, 2017, **9**, 40452–40460.
29 C. C. L. McCrory, S. H. Jung, J. C. Peters and T. F. Jaramillo, *J. Am. Chem. Soc.*, 2013, **135**, 16977–16987.